Materials Advances

ROYAL SOCIETY OF CHEMISTRY

REVIEW

View Article Online
View Journal | View Issue

Cite this: *Mater. Adv.*, 2022, 3, 6728

Metal–organic framework-based photonic crystal platforms for gas sensing: a review

Zhaolong Wang,[a] Yaru Wang,[a] Jun Yan,[a] Bin Liu,[a] Yunlin Chen *[a] and Yahui Tian*[b]

Based on the low cost, high sensitivity and high reliability of photonic crystal (PC) platforms, they stand out in the family of gas sensors for label-free gas detection. Numerous breakthroughs have been achieved in terms of response speed, selectivity and specificity by integrating MOFs in PC sensors as functional materials, resulting in the formation of metal-organic framework (MOF)-based PC gas sensors. Due to the combination of the photonic band gap (PBG) of PCs with the specific properties of MOFs, such as tunable structure, diversity, large porosity and high specific surface area, tremendous progress has been made in the past decade on MOF-based PC gas sensors with high sensitivity and selectivity. However, although there are several reviews in the literature summarizing the use of MOFs as gas sensors, a comprehensive review focusing on MOF-based PC gas sensors from 1-dimensional (1-D) to 3-D PCs is lacking. In this review, the research progress on MOF-based PC gas sensors from 1-D to 3-D PCs, which mainly include four aspects of sensing mechanism, material selection, structural optimization and sensing performances, is comprehensively summarized. Firstly, an overview of the corresponding sensing principle for PC sensors is presented. Further, the sensing properties such as sensitivity, response and recovery time, limit of detection (LOD), selectivity, and repeatability of various MOF-based PC sensing systems are illustrated and discussed. Finally, a summary and outlook of MOF-based PC gas sensors are presented to pave the way for their practical applications.

Received 8th March 2022,
Accepted 9th July 2022

DOI: 10.1039/d2ma00269h

rsc.li/materials-advances

Introduction

The real-time monitoring of various flammable, explosive, toxic and harmful gases has become increasingly important for industrial manufacture, environmental protection, household security, agriculture, medical diagnosis, food supervision, *etc.*[1–5] In particular, environmental issues have increased globally.[6,7] Nature, the environment in which human beings live, has been damaged significantly. Formaldehyde, ammonia (NH_3), hydrogen sulfide (H_2S), nitrogen oxide (NO_x), sulfur oxide (SO_x), carbon oxide (CO_x) and other volatile organic chemical (VOC) vapors from industrial processes and building materials pose a major threat to humans and the environment.[8–16] This increases the need for environmental monitoring systems such as the internet of things (IOT) for environmental protection. Gas sensors, as essential sensors for environmental monitoring, will help build environmental IOT.[17]

Various types of gas sensing technology have flourished over the past decades, which have played a key role in human life. At present, the gas sensing methods can be classified as gas sensors based on electrical variation,[18–20] optical sensors,[21,22] mass-sensitive sensors,[7] and other sensors (such as gas chromatograph)[23] according to their sensing mechanism. In the case of gas sensors based on electrical variation such as semiconductor sensors and electrochemical sensors, they have high sensitivity and a low limit of detection (LOD), which can reach the part per billion level.[24] However, they operate at high temperatures and are expensive, restricting their application.[4] In addition, their high power consumption and environmental restrictions such as radiation and high electric/magnetic fields are also problems hindering their progress.[25] Mass-sensitive sensors such as quartz crystal microbalance (QCM) sensors possess high sensitivity and can work at room temperature.[26] However, they are similarly unsuitable because they are affected by radiation or high electric/magnetic fields.[27] Gas chromatographs, which require trained professionals for their manipulation, tend to be large and costly, and thus their use is not widespread.[23,28] Different from gas sensors based on electrical variation, optical sensors, which employ optical transduction techniques to gain sensing signals, have greater security. They can resist electromagnetic interference from radiation or high electric/magnetic fields.[4,21] The optical transduction techniques include optical absorption,[21] luminescence,[29]

[a] *Institute of Applied Micro-Nano Materials, School of Science, Beijing Jiaotong University, Beijing 100044, China. E-mail: ylchen@bjtu.edu.cn*
[b] *Institute of Acoustics, Chinese Academy of Sciences, Beijing 100190, China. E-mail: tianyahui@mail.ioa.ac.cn*

colorimetric,[30,31] and other methods based on the variation in optical parameters such as refractive index.[32,33] Label-free photonic crystal (PC) sensors stand out among the various types of sensors due to their straightforward, precisely controllable and higher sensing performances.[4,25,34] Photonic crystals, which are a type of periodic arrangement of regularly shaped materials, possess a periodic variation in their dielectric constants in the 1-, 2-, or 3-dimensional (1-, 2-, or 3-D) direction.[1,4,35] This periodic arrangement of dielectric constants can form a photonic band gap (PBG) which can forbid the electromagnetic wave of a certain frequency, resulting in the formation of structural colors.[36–39] Moreover, the optical properties of PCs such as the location of their PBG can be modulated readily when exposed to external gas. These performances make PCs very competitive in the sensing field.[40] However, sensors based on PCs are very exciting, but they also have limitations, which cannot precisely identify analytes at the part per billion level.[41]

Accordingly, a promising strategy to enhance the sensing properties of PC sensors is their combination with new gas-sensitive materials. Optical sensors consisting of metal–organic frameworks (MOFs) have thrived in the last decade since the groundbreaking work published by J. T. Hupp *et al.*[42] Metal–organic frameworks, also known as crystalline inorganic–organic hybrid porous materials, are ordered structures composed of metal ions and organic ligands.[5,43–47] As a type of advanced porous material, MOFs have numerous advantages in photonic and electronic devices and energy storage fields.[48–50] Firstly, the ordered structures of MOFs, which are affected by the coordination geometry of their metal and organic ligands, ensure their thermal and chemical endurance. Meanwhile, their regular network structures also create large specific surface areas. Secondly, the intrinsic optical and electrical performances of MOFs can be tuned because of the flexible adjustability of their components, reticulations, and topological structures.[51] Due to the above-mentioned two reasons, PC gas sensors based on MOFs demonstrate superior sensing performances compared with conventional amorphous nano-porous materials and polymers. With regard to MOF-based PC sensors, their sensing performances including sensitivity, selectivity, response and recovery time, and repeatability are mainly related to the adsorption behaviour of the analyte molecule in the internal surface of the MOFs.[52,53] MOF materials with high porosity exhibit excellent gas sensitivity because they can internally compress the concentration of gas molecules to exceed that in the external environment. The sensitivity is largely determined by the bond strength between the MOFs and analyte, and the dynamic transmission of the analyte molecule in MOFs. The sensitivity and selectivity can also be improved by selecting MOFs with size-exclusion capacity and specific interaction.[54] The size-exclusion effect, also called the molecular sieve effect, can cause MOFs to adsorb molecules or atoms that are smaller than their pore diameter. The size-exclusion effect depends on the porosity of MOF materials and their organic ligands and metal ions. The selectivity of MOFs may originate from the interaction of the analyte with their organic ligands or metal ions. The specific interaction such as hydrogen bonds or coordinate covalent bonds between the analyte and MOFs also affect their selectivity. If some analytes interact with the metal ions in MOFs, they may be preferentially adsorbed. In addition, the response time is also a significant parameter for a sensor. The size, shape, and properties of the pores in MOFs are directly related to the adsorption kinetics, which strongly influence the generated signal and the rate of signal transmission. The response rate depends on the adsorption kinetics, which is controlled by the dynamics of the analyte transport in MOFs, *i.e.*, the rate of diffusion of guest molecules in the MOF particles or films.[3] Moreover, the repeatability of sensors also depends on the kinetics and thermodynamic processes of adsorption in MOFs, given that the adsorption of most guest molecules is a physical adsorption process.

The recent reviews in the literature discussed the types of MOF-based chemical sensors, the classification of analytes, the role of MOFs in sensors, and their preparation and synthetic methods.[3,55,56] The development and prospect of MOF materials used in sensors are described in detail in these reviews. However, they broadly discussed the application of MOF materials in chemical sensors and there is no specific review describing the application of MOF materials in PC gas sensors from 1-D to 3-D PCs. Thus, the aim of the present review is to provide a complementary overview of the latest research on MOF integration in PC sensors.

To promote the practical use of MOF-based PCs in gas sensing, herein, we present a review covering MOF-based PCs from 1-D to 3-D PCs as gas sensors in environmental protection (Fig. 1). This review summarizes the development of MOF-based PC gas sensors. Firstly, we explain the optical characteristics and sensing principle of PC sensors, which offers theoretical reference for researchers beyond the PC sensor community.

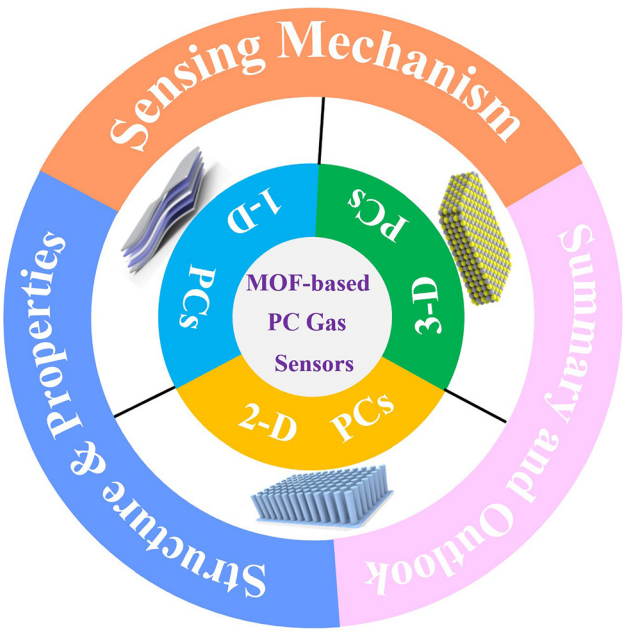

Fig. 1 Schematic diagram of the classification of MOF-based PC gas sensors in this review.

Subsequently, we overview the key progress in gas detection using MOF-based PC sensors. The device architectures of MOF-based gas sensors are comprehensively discussed. In particular, in this review, we discuss the MOF-based 1-D PC gas sensors with easily predicted optical performances, MOF-based 2-D PC gas sensors demonstrating excellent sensitivity and response, and MOF-based 3-D PC gas sensors with sensing units that can be customized. Concurrently, the interactions in MOF and PC sensors are discussed, which include the relationship between adsorption characteristics of MOFs and sensing properties of PC sensors such as sensitivity, selectivity, stability, response and recovery time, repeatability and LOD. Finally, we present a summary and prospects of MOF-based PC gas sensors for further development and practical application.

Sensing mechanism of PC sensors

In the late 1980s, E. Yablonovitch and S. John presented the concept of PCs, and subsequently the research on PCs intensified.[57,58] PCs are periodically optical nanomaterials. The movement track of photons in PCs is similar to the motion of electrons in semiconductors.[59–61] According to periodic variation in the dielectric constants in the 1-, 2-, and 3-D directions, they can be classified as 1-, 2-, and 3-D PCs, respectively (Fig. 2). 1-D PCs (Bragg-Stacks) are multiple-layer structures assembled by alternating layers of two materials with high and low refractive indices. This means that 1-D PCs show a regular variation in their refractive index in one direction but are isotropic in the other two directions.[62,63] 2-D PCs have periodically varied refractive indices in two directions but homogenous in the third direction. 3-D PCs are structures in which the refractive index regularly varies in all three directions.

The dispersion relationship of light propagation in free space can be depicted as follows:[1]

$$w = ck \tag{1}$$

where w is the frequency, c is the velocity of light under vacuum, and k is the wave vector. Analogously, the dispersion relationship of electron propagation in a homogeneous medium can be depicted as follows:[1]

$$w = (k^2h)(4\pi m) \tag{2}$$

where h and m are Planck's constant and mass of an electron, respectively. According to eqn (1) and (2), the frequency, w, and wave vector, k, are linearly related to the dispersion relation of light, while w and k are quadratic-dependent in the dispersion relation of electronics. The wavelength of waves associated with electrons is much smaller than that of photons.[1] This implies that the periodic arrangement of atoms in crystals will be seen as a homogeneous medium by visible light and lattice constants of several hundreds of nm are required to have an effect on light.[1] When exposed to a periodical structure, the propagation of electromagnetic waves can be given by Bragg's law,[34,64,65] as follows:

$$m\lambda = 2n_{\text{eff}}d\sin\theta \tag{3}$$

where m, λ,..., d, and θ are the diffraction order, wavelength of incident electromagnetic waves, effective refractive index, interplanar crystal spacing, and incident angle, respectively. Likewise, when visible light is incident in the periodic structure with a regular change in the dielectric constant such as PCs, the Bragg's law also holds.[64] Only the meaning of λ is changed from the wavelength of incident light to the maximum reflection peak of $\lambda_{\max}$. Given the above-mentioned facts, as visible light penetrates normal PCs, the maximum reflection peak can be tuned by the variation in the effective refractive index and the interplanar crystal spacing. Therefore, as long as the analyte can induce a change in the spacing lattices or the refractive index in PCs, the shift of the maximum reflection peak can serve as a sensing signal to detect the analyte. According to the effective medium theory, the effective index can be given by the following formula:

$$n_{\text{eff}}{}^2 = \sum n_i^2 v_i^2 \tag{4}$$

where n_i is the refractive index of the independent components in PCs and v_i represents the volume fraction of independent constituents. Moreover, light of a specific wavelength or frequency will be reflected due to the PBG in PCs. Similarly, the structure color will change when the maximum reflection peak changes, which also can be used as a sensing signal.

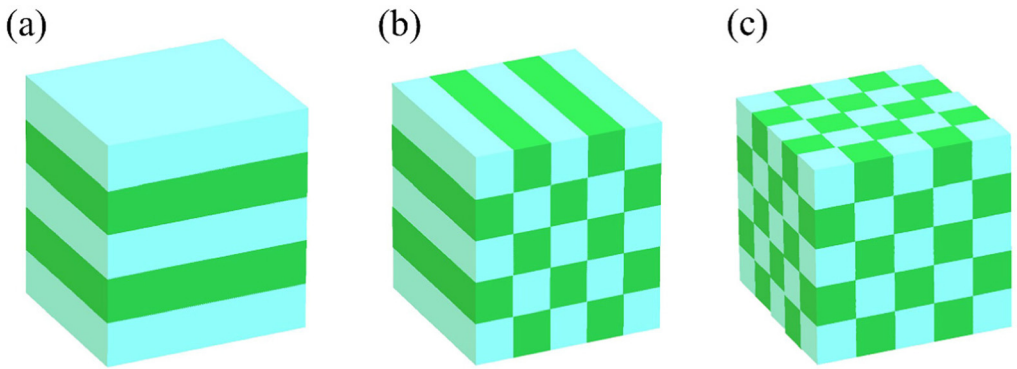

Fig. 2 Schematic of 1-D (a), 2-D (b), and 3-D (c) PCs.

MOF-based 1-D PC gas sensors

1-D PCs are composite structures that are alternately assembled by high and low reflective materials. Therefore, at normal incidence, Bragg's law, which depicts the diffraction characteristics of 1-D PCs, can be transformed into the following formula:[66]

$$m\lambda_{max} = 2(n_L d_L + n_H d_H) \quad (5)$$

where n_L and n_H are the reflective index of low and high reflective materials and d_L and d_H are the thickness of low and high reflective materials, respectively. The reflectivity of R also can be given by the following formula:[67]

$$R = \left[\frac{n_0 - n_s\left(\frac{n_L}{n_H}\right)^{2N}}{n_0 + n_s\left(\frac{n_L}{n_H}\right)^{2N}}\right]^2 \quad (6)$$

where N is the periodic number of 1-D PCs and n_s and n_0 are the reflective index of the substrates and ambient environment, respectively. Moreover, the bandwidth $\Delta\lambda_{max}$ of the PBG can be estimated using eqn (7),[64] as follows:

$$\Delta\lambda_{max} = \frac{4\lambda_{max}}{\pi}\arcsin\left(\frac{n_H - n_L}{n_H - n_L}\right) \quad (7)$$

Several conclusions also can be drawn from the theory described above. Firstly, 1-D PCs have simple structures and their optical performances can be easily predicted.[68] Secondly, 1-D PCs, which are prepared by using MOFs as low reflective index layers, demonstrate adjustable reflectivity. The adjustable reflectivity is mainly due to the pore environments of MOFs, which can be precisely tuned. In addition, 1-D PCs are easy to prepare due to their simple structure. In this section, we only focus on MOF-based 1-D PCs for gas sensing. Table 1 summarizes the MOF-based 1-D PC gas sensors according to their components, target analytes, sensitivity, response and recovery time, and LOD.

The work principle of MOF-based 1-D PC gas sensors depends primarily on the specific adsorption of gas molecules on MOFs. The specific adsorption can change the refractive index of PCs, and thus transduces the recognition events into detectable optical signals. The specific interactions between MOFs and gas molecules include van der Waals forces, hydrogen bonding, and π–π interactions. Therefore, the choice of MOFs is very important to detect specific gas molecules. Moreover, for a sensor, its normal operation in different environments is also a requirement. There are higher requirements for thermal and chemical stability. Thus, MOFs with excellent mechanical, thermal and chemical stability can be potential candidates, such as zeolitic imidazolate framework-8 (ZIF-8). In addition, a high refractive index contrast is required to acquire a regular variation in refractive index in one direction. According to this strategy, B. V. Lotsch and J. T. Hupp reported parallel work in the fabrication of MOF-based 1-D PC gas sensors.[69,70] B. V. Lotsch *et al.* utilized TiO_2 and ZIF-8 as high and low reflective index layers to prepare 1-D PC gas sensors (Fig. 3a). Based on the strong adsorption capability of ZIF-8, the 1-D PC sensors had an obvious optical response to ethanol and methanol. J. T. Hupp and co-workers prepared a 1-D PC film consisting of different numbers of Pd/ZIF-8 bilayers. Fig. 3b shows the cross-sectional scanning electron microscopy (SEM) image of the Pd/ZIF-8 1-D PC gas sensor. The composite film assembled by two cycles of Pd/ZIF-8 bilayers exhibited obvious shifts in its transmission peak when exposed to ethane, ethylene, propane, and propylene. Moreover, the increasing transmittance of the 1-D PC film could be observed in an H_2 atmosphere because of the interaction between Pt and H_2. 1-D PC gas sensors based on rigid MOFs such as ZIF-8 usually demonstrate excellent stability. However, the variation in their refractive index due to absorbing vapor is limited. The shifts in the maximum reflected peaks are not significant, even in saturated steam environments, which is not suitable for high-sensitivity sensing applications. This problem can be improved with the use of flexible MOFs as the adsorption layer. Layer expansion can be achieved for flexible MOFs by gas adsorption, resulting in an obvious change in their optical thickness and refractive index. In 2014, J. Wang *et al.* reported a simple spin-coating method to fabricate MOF photonics films (Fig. 3c), and subsequently they systematically studied the effect of solution concentration, rotating speed, and rotating cycles on the thickness and optical quality of the films.[71] The NH_2-MIL-

Table 1 Comparison of sensing performances of different MOF-based 1-D PC gas sensors

Components	Target analyte	Sensitivity	Response time	Recovery time	LOD	Ref.
ZIF-8/TiO_2	Ethanol	100 nm (Saturated vapor)	—	—	—	70
ZIF-8/Pt	Ethanol/H_2	~90 nm (Saturated vapor)	—	—	—	69
NH_2-MIL-88B	Acetone	380 nm (Saturated vapor)	>2 min	—	—	71
NH_2-MIL-88B/TiO_2	Ethanol	66.4 nm (Saturated vapor)	—	—	—	68
HKUST-1/ITO	Toluol	38 nm (Saturated vapor)	—	—	—	74
ZIF-8, HKUST-1, CAU-1-NH_2	Mixed gases	—	5–10 s	5–10 s	—	75
CAU-1/TiO_2	Heptane	~75 nm (Saturated vapor)	~5 s	—	—	76
NH_2-MIL-88B/(P(St-AA))	Xylene	4.3×10^{-3} nm ppm^{-1}	2.5 s	3 s	0.22 g m^{-3}	77
MIL-101-NH_2 (Cr)/TiO_2	Methanal	0.02 nm ppm^{-1}	0.5 s	20 s	5 ppm	78
MIL-801/TiO_2	Humidity	0.1%RH	~2 s	~5 s	15–95%RH	79
ZIF-8@ZnO/TiO_2	Carbon tetrachloride	0.05 nm ppm^{-1}	~300 ms	4.7 s	—	82
ZIF-8(Zn@Co)/TiO_2	Chlorobenzene	0.05 nm ppm^{-1}	0.6 s	9.5 s	6.92 ppm	84
TiO_2/UIO-66/GO	Chlorobenzene	0.03 nm ppm^{-1}	800 ms	5 s	13 ppm	41
MIL-101 (Cr)/TiO_2	Carbon tetrachloride	0.11 nm ppm^{-1}	1.2 s	12.1 s	0.89 ppm	67
UIO-66-NH_2/TiO_2	HCl	1.19% ppm^{-1}	1 s	8 s	220 ppb	86

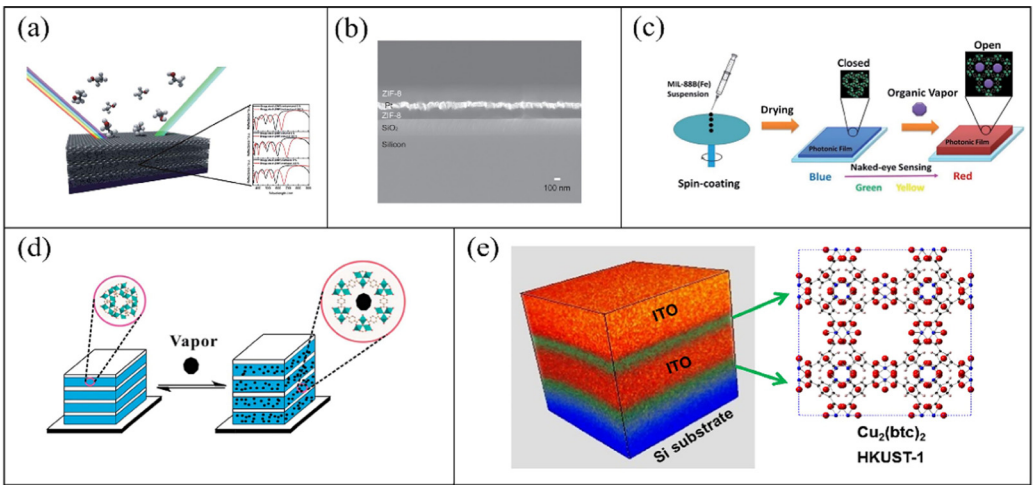

Fig. 3 (a) Schematic illustration of the ZIF-8/TiO_2 1-D PC gas sensor. Reproduced with permission.[70] Copyright 2012, The Royal Society of Chemistry. (b) Cross-sectional SEM image of the ZIF-8/Pt 1-D PC gas sensor. Reproduced with permission.[69] Copyright 2012, Wiley-VCH. (c) Schematic diagram of the fabrication of NH_2-MIL-88B photonic film. Reproduced with permission.[71] Copyright 2014, The Royal Society of Chemistry. (d) Schematic diagram of NH_2-MIL-88B/TiO_2 1-D PC gas sensor. Reproduced with permission.[68] Copyright 2014, The Royal Society of Chemistry. (e) Schematic of HKUST-1/ITO 1-D PC gas sensor. Reproduced with permission.[74] Copyright 2015, the American Chemical Society.

88B MOF was used for as sensitive material due to its exceptional structural flexibility. A framework with structural flexibility can undergo large expansion without obvious bond destruction in the analyte environment ("breathing" effect).[72,73] The reflective peak of the simple photonic film showed an apparent red-shift of 380 nm and a significant variation in structural color when exposed to acetone vapors at saturated vapor pressure. This sensor exhibited a response time of 2 min and good repeatability due to the flexible structure of NH_2-MIL-88B. In the same year, based on previous research, J. Wang *et al.*[68] fabricated a flexible MOF-based 1-D PC gas sensor consisting of TiO_2 and NH_2-MIL-88B *via* a spin-coating method (Fig. 3d). The TiO_2 layers ensured high reflective contrast and the NH_2-MIL-88B layers were used as intrinsic functional layers. Due to the fast kinetics of breathing in the presence of EtOH, the 1-D PC gas sensor had maximum red-shifts in its reflective peak for EtOH vapors. Meanwhile, the high thermal and mechanical stability guaranteed the long-term application of the NH_2-MIL-88B-based 1-D PC sensor. In addition, the choice of high refractive index layers with high optical quality such as indium tin oxide (ITO) also produced high PBG reflectivity. E. Redel *et al.*[74] reported the preparation of a 1-D PC gas sensor consisting of HKUST-1 by liquid phase epitaxy (LPE) and ITO deposited by a sputtering method in 2015 (Fig. 3e). The unique components of the HKUST-1/ITO 1-D PCs resulted in a high PBG reflectivity of 80%. Again, the HKUST-1/ITO 1-D PC sensor exhibited the maximum PBG shifts in toluene vapors.

To enhance the selectivity of sensors, innovative manufacturing strategies and the advanced data-analyzing methods are essential. Although single sensing units play a prominent role in gas detection, they are unsuitable for the detection of mixed gases. Furthermore, target gases frequently contain analytes dispersed in various phases (for example, air, organic and aqueous), thus making the identification of chemical species a challenge. Accordingly, sensing arrays integrating multiple sensing units can overcome this issue. Sensing arrays can accurately distinguish different gases with the help of intelligent algorithms. B. V. Lotsch *et al.*[75] utilized TiO_2 and MOFs (ZIF-8, HKUST-1, and CAU-1-NH_2) to prepare three 1-D PC sensors (Fig. 4a(i)). The TiO_2/MOFs (ZIF-8, HKUST-1, and CAU-1-NH_2) demonstrated both high selectivity and sensitivity to ethanol and methanol and rapid response times. As is shown in Fig. 4a, B. V. Lotsch and co-workers developed two different strategies to obtain a high-level specificity. In the first method, they combined ZIF-8 layers with either CAU-1-NH_2 or HKUST-1 layers to prepare tandem MOF 1-D PCs. The results of the sorption isotherms showed the enhanced analyte specificity of the tandem MOFs (ZIF-8/HKUST-1 and ZIF-8/CAU-1-NH_2). In the other method (Fig. 4a(ii)), they prepared a sensing array assembled using TiO_2/MOFs (ZIF-8, HKUST-1, and CAU-1-NH_2). The sensing array possessed a combinatorial response, where each part showed a unique signal to improve analyte specificity. The variation in the structural color of the sensing array with host–guest interactions could be used as an analyte-specific fingerprint. This fingerprint was analyzed through principal component analysis (PCA) to realize the classification of gas mixtures. Subsequently, B. V. Lotsch and A. von Mankowski[76] also reported a method to enhance the analyte selectivity by post-assembly modification of CAU-1-based 1-D PC sensors (Fig. 4b(i)). The post-assembly modification, which changed the coordination environments of the metal–oxo secondary building unit or formed an amide at the linker, affected the adsorption behaviors and host–guest interactions of the CAU-1-based 1-D PC sensor (Fig. 4b(ii)). The post-assembly modification strategy can fine-tune the performances of the MOF layers. Therefore, the selectivity and sensitivity of the CAU-1-based 1-D PC sensors could be fine-tuned. Similarly, the color images of the sensors were evaluated by PCA with analyte environments, thereby realizing the classification of different gas. In addition,

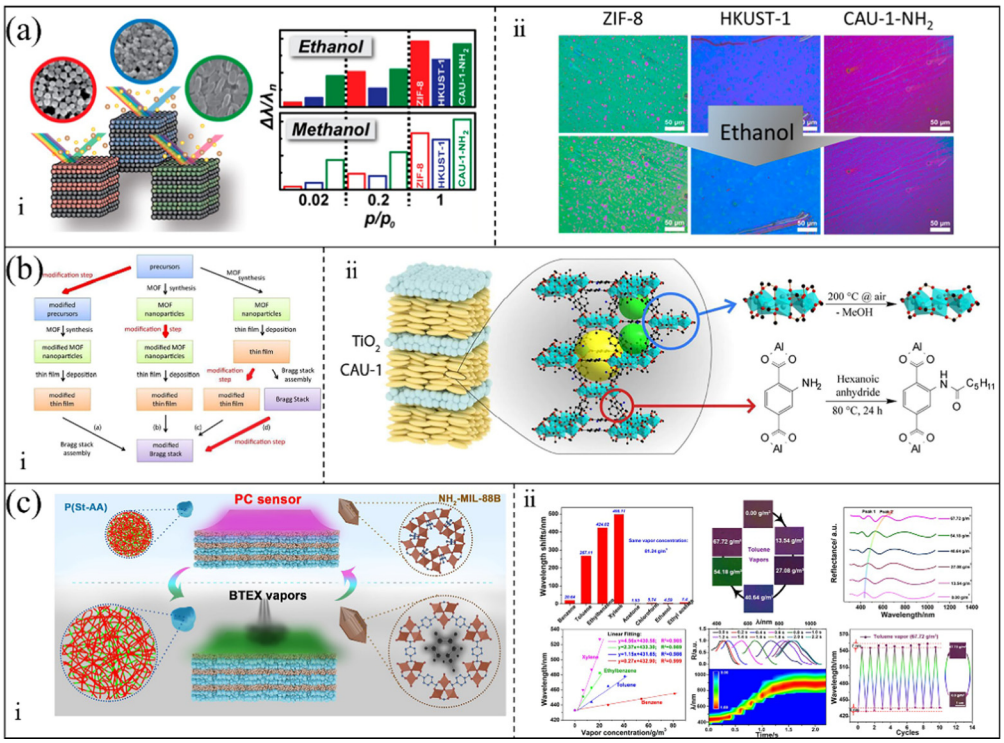

Fig. 4 (a) i Schematic diagram of TiO_2/MOF (ZIF-8, HKUST-1, and CAU-1-NH_2) 1-D PC gas sensors. ii Color change in a sensing array assembled by TiO_2/MOFs (ZIF-8, HKUST-1, and CAU-1-NH_2) when exposed to ethanol vapor. Reproduced with permission.[75] Copyright 2015, the American Chemical Society. (b) i Representation of the key steps during the fabrication of 1-D PCs and the modification step. ii Schematic of the post-assembly modification of CAU-1/TiO_2 1-D PC gas sensor. Reproduced with permission.[76] Copyright 2018, The Royal Society of Chemistry. (c) i Schematic illustration of NH_2-MIL-88B/P(St-AA) 1-D PC gas sensor when exposed to benzene, toluene, ethylbenzene, and xylene vapors. ii Sensing of the NH_2-MIL-88B/P(St-AA) 1-D PC gas sensor. Reproduced with permission.[77] Copyright 2020, the American Chemical Society.

W. Ma *et al.*[77] integrated an MOF and a polymer to fabricate a 1-D PC gas sensor assembled by NH_2-MIL-88B layers and poly(styrene-acrylic acid) (P(St-AA)) layers. Through the "breathing" effect of flexible NH_2-MIL-88B and (P(St-AA)), this sensor could realize the recognition of benzene, toluene, ethylbenzene, and xylene (Fig. 4c(i)). The LOD for benzene, toluene, ethylbenzene, and xylene reached 3.70, 0.87, 0.42, and 0.22 g m^{-3}, respectively.

Meanwhile, as shown in Fig. 4c(ii), the 1-D PC sensor showed a response time of 3 s and rapid recovery due to its porous and super-thin structure.

To improve the selectivity of MOF-based 1-D PC sensors and acquire a higher detection level, the selection of new MOFs with excellent specificity and their combination with other gas-sensitive materials such as metallic oxides or graphene can be a promising strategy. Recently, Y. Chen's group reported their studies on MOF-based 1-D PC gas sensors. As depicted in Fig. 5a, Y. Chen and Y. Xing[78] prepared an MOF-based 1-D PC methanal sensor composed of MIL-101-NH_2 (Cr) and TiO_2 *via* a spin-coating method. The methanal sensor had a high concentration sensitivity of ~0.02 nm ppm^{-1} and LOD of 5 ppm. Meanwhile, the methanal sensor exhibited reliable repeatability and stability. Y. Chen *et al.*[79] also utilized MIL-801-based 1-D PCs to realize the sensing of humidity (Fig. 5b). Due to their large pores and high specific surface area,[80,81] the 1-D PCs exhibited good sensing performances for water vapor. The sensor had a rapid response time of 2 s and excellent repeatability and reliability. The introduction of defect layers in PCs can change their adsorption properties, which also can be an innovating way to achieve the sensing of analytes. Y. Chen and K. Zhan[82] reported a 1-D PC sensor with top-defects based on ZIF-8@ZnO/TiO_2. The ZIF-8@ZnO sol was added on the top of the native ZIF-8/TiO_2 1-D PC (Fig. 5c). The adsorption characteristics of ZnO were positively related to the molecular weight but negatively correlated with the dipole moment, which enhanced the sensing ability of the ZIF-8@ZnO/TiO_2 1-D PC gas sensor to carbon tetrachloride.[83] The tetrachloromethane sensor exhibited a high concentration sensitivity of 0.05 nm ppm^{-1} and response and recovery time of 300 ms and 4.7 s, respectively. Subsequently, they also proposed a bimetallic MOF-based (ZIF-8(Zn@Co)/TiO_2)n 1-D PC chlorobenzene sensor and optimized its structure with the transfer matrix method (Fig. 5d).[84] Co^{2+} could improve the chemical heterogeneity of the framework and micro-porosity of ZIF-8(Zn@Co), thereby enhancing its adsorption capacity.[85] Meanwhile, the π–π interactions between the imidazolate linkers of the frameworks and the benzene ring also enhanced the absorption of chlorobenzene. Therefore, this sensor had a high concentration sensitivity of 0.05 nm ppm^{-1} and low LOD of 6.92 ppm. Likewise, in 2021, Y. Chen and Z. Wang[41] reported a 1-D PC chlorobenzene sensor assembled using TiO_2, UIO-66 and graphene oxide (GO) (Fig. 5e). The functional layers of GO can provide strong π–π bond interactions with chlorobenzene. Thus, the selectivity of the 1-D PC sensor assembled using TiO_2, UIO-66

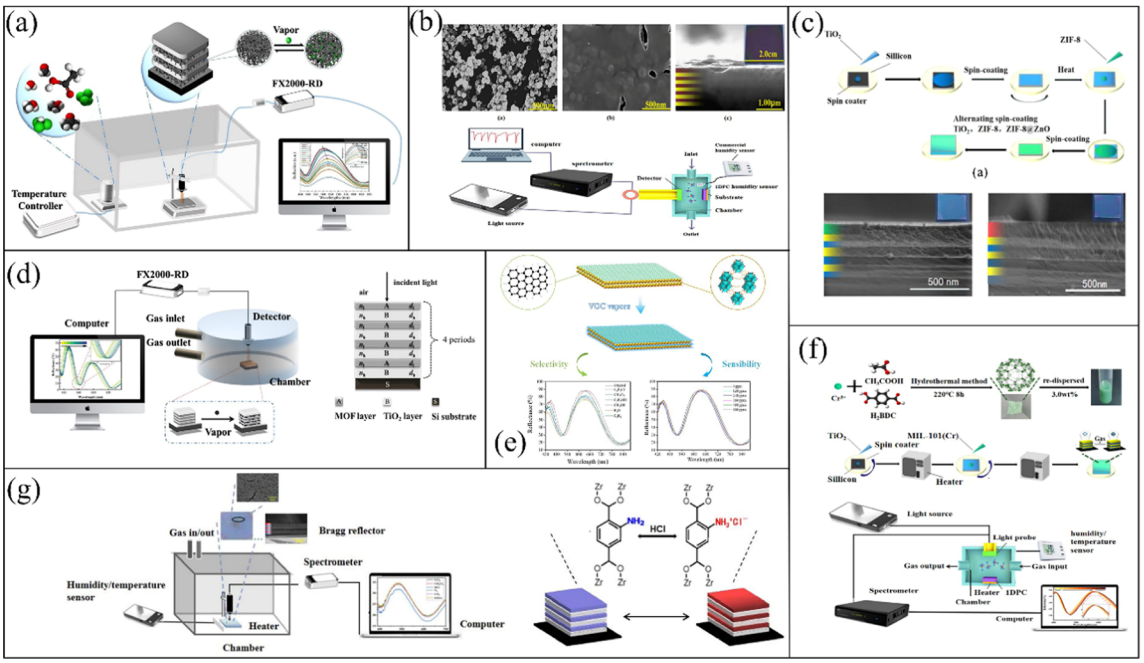

Fig. 5 (a) Sensing system schematic of MIL-101-NH_2 (Cr)/TiO_2 1-D PC methanal sensor. Reproduced with permission.[78] Copyright 2020, Wiley-VCH. (b) Schematic of MOF-801/TiO_2 1-D PC gas sensor. Reproduced with permission.[79] Copyright 2020, Elsevier B.V. (c) Preparation process of ZIF-8/TiO_2 1-D PC sensor. Reproduced with permission.[82] Copyright 2020, Elsevier B.V. (d) Schematic illustration of ZIF-8(Zn@Co)/TiO_2 1-D PC sensing system. Reproduced with permission.[84] Copyright 2021, Elsevier B.V. (e) Schematic diagram of a 1-D PC sensor assembled by TiO_2, UIO-66 and GO. Reproduced with permission.[41] Copyright 2021, Elsevier Ltd. (f) Process for the fabrication of MIL-101(Cr)/TiO_2 1-D PC gas sensor. Reproduced with permission.[67] Copyright 2021, Elsevier Inc. (g) Schematic of UIO-66-NH_2/TiO_2 1-D PC HCl sensor. Reproduced with permission.[86] Copyright 2021, IEEE.

and GO for chlorobenzene vapor was enhanced. In June of the same year, Y. Chen and K. Zhan[67] prepared MIL-101(Cr) *via* a hydrofluoric acid-free method and fabricated MIL-101(Cr)/TiO_2 1-D PCs to realize the sensing of CCl_4 vapor (Fig. 5f). In addition, they also utilized UIO-66-NH_2 and TiO_2 to fabricate a 1-D PC HCl sensor.[86] There are two main reasons for the excellent selectivity of the UiO-66-NH_2/TiO_2 sensor for HCl. On the one hand, the van der Waals forces between the polar UiO-66-NH_2 and the polar HCl caused the UIO-66-NH_2/TiO_2 sensor to have strong sensitivity. On the other hand, as is illustrated in Fig. 5g, the HCl and amine group in UIO-66-NH_2 can form an ammonium chloride adduct, thereby enhancing the selectivity for HCl. Hence, the LOD of the UIO-66-NH_2/TiO_2 sensor to HCl vapor reached as low as 220 ppb.

MOF-based 2-D PC gas sensors

2-D PC structures are ordered lattices, which can be created by a regular row of holes, wires, rods, and tubes.[87,88] Their unique characters such as photon localization make them rapidly evolve in the field of physics, chemistry, biology, materials science, nanotechnology, *etc.*[89–92] Compared with 1-D and 3-D PC sensors, 2-D PC sensors required a small amount of different materials and a thin overall structure, result in excellent sensitivity and response.[52] Thus, it is significant to prepare 2-D PCs for the design of outstanding-performance MOF-based 2-D PC gas sensors.[75] A variety of methods for the preparation of MOF-based 2-D PCs has been reported, including template-assisted methods, photolithography technologies, and other methods. D. Chen and C. Li[52] proposed the use of an ultrathin MOF-based monolayer colloidal crystal for vapor sensing. As is illustrated in Fig. 6a(i), the MOF-coated monolayer colloidal crystals were prepared *via* two procedures. Firstly, monolayer colloidal crystals consisting of polystyrene (PS) spheres were prepared *via* self-assembly at the air–water interface. Next, an ultrathin ZIF-8 film was growth on the surface of the monolayer colloidal crystals *via* a modified cyclic growth method. The ZIF-8-coated monolayer colloidal crystals exhibited two optical modes, *i.e.*, 2-D PCs and Fabry–Pérot oscillations, which had an excellent selective response to a series of alcohols and acetonitrile (Fig. 6a(ii)). The sensitivity of the sensor was closely related to the thickness of the MOF film. In addition, the sensor also demonstrated a fast response time of less than 5 s and remarkable repeatability. The next year, D. Chen *et al.*[93] also reported the preparation of an MOF-based optical sensor, which was a hollow MOF nanoshell-based etalon. The process for the preparation of the sensor is shown in Fig. 6b. Firstly, the monolayer colloidal crystals assembled by PS spheres were deposited on the surface of silicon wafers. Secondly, silicon wafers with monolayer colloidal crystals were put in solution to coat the ZIF-8 film. Next, the ZIF-8-based monolayer colloidal crystals assembled by PS spheres were dipped in dichloromethane to remove their PS core. Finally, a thin Pt layer was sputtered on the hollow MOF nanoshell-based etalon to enhance the structural colors. The sensor exhibited an excellent response to a series of alcohols and a distinct difference between benzene and cyclohexane. Meanwhile, due to the ultrathin

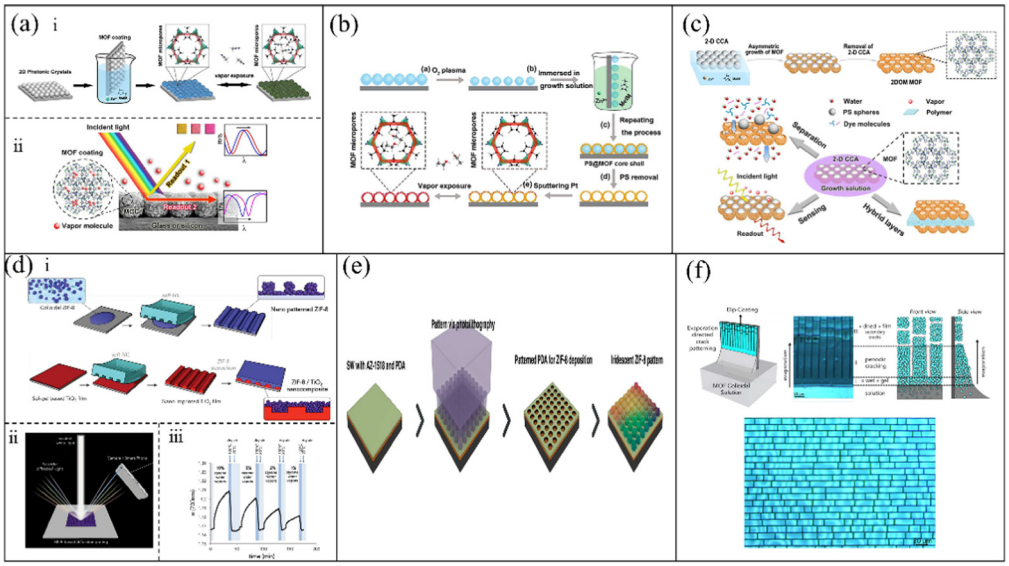

Fig. 6 (a) i Process for the fabrication of an ultrathin ZIF-8-coated 2-D PC gas sensor. ii Schematic illustration of dual-sensing signal of the ZIF-8-coated 2-D PC gas sensor. Reproduced with permission.[52] Copyright 2015, the American Chemical Society. (b) Schematic of the fabrication of the hollow MOF nanoshell-based 2-D PC VOC sensor. Reproduced with permission.[93] Copyright 2016, Wiley-VCH. (c) Schematic of ZIF-8-based 2-D colloidal crystal arrays. Reproduced with permission.[94] Copyright 2016, the American Chemical Society. (d) i Process for the fabrication of 2-D PC sensing arrays with nanopatterned ZIF-8 and ZIF-8/TiO_2 heterostructures. ii Illustration of a detecting experiment platform using a smart phone. iii Sensitive detection using ZIF-8 colloidal film when exposed to varying styrene/water vapors. Reproduced with permission.[95] Copyright 2016, Wiley-VCH. (e) Procedure for the preparation of an iridescent ZIF-8 2-D PC array. Reproduced with permission.[96] Copyright 2017, the American Chemical Society. (f) Schematic of the dip-coating assisted crack-pattering process. Reproduced with permission.[97] Copyright 2017, Wiley-VCH.

nanoshells and the hollow monolayer structures, the sensor showed a rapid response time of less than 2 s. In addition, D. Chen and C. Li[94] presented a method for the fabrication of a multi-function MOF-based superstructure based on previous research (Fig. 6c). Firstly, ZIF-8 precursor solutions were prepared. Secondly, the 2-D colloidal crystal array assembled by PS spheres was anchored at the air-solution interface of the ZIF-8 precursor solutions. Next, the ZIF-8 films were asymmetrically grown on a 2-D colloidal crystal array. Finally, the 2-D ordered macroporous MOF films were acquired by removing the cores of the 2-D colloidal crystal arrays. Compared with unstructured MOF films, the 2-D ordered macroporous MOF films showed brilliant performances in the fields of gas sensing, size-screening of nanoparticles, and removal of dye molecules from aqueous solutions.

A. Cattoni and Marco Faustini[95] described a soft-lithographic method for the fabrication of MOF-based 2-D PCs on the micro-scale. As is depicted in Fig. 6d(i), a nanopatterned ZIF-8 film and ZIF-8/TiO_2 heterostructure were prepared. One nanopatterned ZIF-8 film was prepared *via* soft-lithographic technology. The other ZIF-8/TiO_2 heterostructure was produced by depositing ZIF-8 films on the pre-prepared TiO_2 films. The pattern of the TiO_2 films was prepared by soft-lithographic technology. Combined with a smartphone camera (Fig. 6d(ii)), the sensing system could selectively detect styrene in the presence of interfering water. Fig. 6d(iii) shows the variation in the refractive index of the nanopatterned ZIF-8 system in different styrene concentrations. The LOD of the nanopatterned ZIF-8 system was as low as 57 ppm. Likewise, A. Razmjou *et al.*[96] utilized photolithography techniques to prepare patterns on the surface of polydopamine, and then deposited a ZIF-8 film on the surface of polydopamine to acquire a patterned ZIF-8-PDA 2-D PC array (Fig. 6e). The iridescent 2-D PCs exhibited potential applications in sensing and photonics. In addition to the use of template-assisted methods and photolithography technology, M. Faustini *et al.*[97] demonstrated a facile method for the production of periodic crack arrays in an MOF film (Fig. 6f). The MOF film with a periodic array of cracks was employed as a 2-D PC diffraction grating vapor sensor. This sensor could realize the detection of variation vapors due to the selective sorption performances of the MOF materials and the rapid optical response of the 2-D PC diffraction gratings.

MOF-based 3-D PC gas sensors

3-D PCs, such as opals and inverse opals, have periodical changes in their dielectric structure in three dimensional directions.[98] Bottom-up approaches are mainly employed to produce 3-D PCs because the top-down methods for their fabrication 3-are expensive and inefficient.[35,64,99] In the bottom-up methods, the building blocks are usually self-assembled into an ordered structure under the action of specific driving forces. The 3-D PCs prepared *via* bottom-up approaches often demonstrate face-centered cubic (fcc) or hexagonal close-packed (hcp) structures, in which the (111) crystalline plane is parallel with the surface of the substrate. Hence, Bragg's law, which depicts the diffraction characteristics

of 3-D PCs can be transformed into the following formula at the normal incidence:

$$m\lambda = \sqrt{\frac{8}{3}}D\sqrt{{n_{\text{eff}}}^2 - \sin^2\theta} \quad (8)$$

where D is the center-to-center distance between the building blocks (lattice spacing). Compared with other types of optical sensors such as 1-D Bragg-stacks fabricated by spin-coating, 3-D PCs prepared *via* bottom-up approaches have flexibly tailored patterns of sensing units. Consequently, the practical use of 3-D PCs has become widespread. Table 2 also summarizes the characteristics of MOF-based 3-D PC gas sensors according to their components, target analytes, sensitivity, response and recovery time, and LOD.

At present, 3-D PC gas sensors based on MOFs are usually self-assembled *via* bottom-up approaches. In the early reports of 3-D PC gas sensors based on MOFs, they were prepared *via* template-assisted methods. The typical components of the templates are SiO_2 and PS spheres. J. T. Hupp *et al.*[100] fabricated MOF-silica colloidal crystals and verified their sensing performances. HKUST-1 was chosen as the adsorption layer because of its high porosity and large specific surface area. The colloid crystal (the opals structure) template was prepared *via* vertical deposition with silicon dioxide microspheres. The MOF-silica colloidal crystal sensor was established by growing an HKUST-1 ultrathin film on the colloidal crystals based on a step-by-step approach. Fig. 7a shows the SEM picture at low and high magnification. It was observed that HKUST-1 was evenly coated on the surface of the silica colloidal crystal. The HKUST-1-silica colloidal crystal film exhibited high sensitivity to ethanol, carbon disulfide and water. The LOD for ethanol, carbon disulfide and water reached 0.3, 0.5 and 2.6 ppm, respectively. G. Li and F. Li[101] reported the preparation of an MOF-based 3-D ordered colloidal crystal array for gas sensing. The sensing system utilized a PS colloidal crystal array as a template structure. Similarly, the HKUST-1 layer served as the sensing element in situ-coated on the surface of the PS-based opal structure. The route for the fabrication of the HKUST-1-PS colloidal crystal gas sensing system is outlined in Fig. 7b. Based on the structural flexibility and adsorption capacity of the MOF shell, the core–shell structure of HKUST-1 and PS colloidal crystal array showed remarkable selectivity for methanol. Compared with the opal structures, the inverse opal structures showed higher volume fractions (air void of 0.74).[102] Therefore, inverse opal structures are more competitive in the sensing field. G. Li *et al.*[103] demonstrated the fabrication of an HKUST-1-based photonic film with an inverse opal structure. The fabrication process is illustrated in Fig. 7c. The precursor solution of HKUST-1 was infiltrated in a PS opaline template and heated to undergo crystallization. The 3-D ordered inverse opal structure gas sensor was obtained be removing the PS template. The 3-D ordered inverse opal film exhibited obvious spectral shifts of ultraviolet-visible (UV-Vis) for ethanol and rapid response. In addition, G. Li *et al.*[104] proposed a general strategy for the preparation of MOF-based 3-D PCs, which utilized spherical PCs as the host templates (Fig. 7d). The PC spheres were fabricated *via* the droplet-based microfluidic technique. The PC spheres demonstrated a high diffusion flux and homogeneous photonic properties, where their structural color was independent of the angular variation. In their work, four different MOF materials (HKUST-1, MOF-5, ZIF-8, and MIL-100) were coated on the surface of the PC spheres. Label-free MOF-based 3-D PC sphere arrays for the detection and discrimination of organic vapor were obtained by arranging these MOF-based photonic spheres. However, the research on MOF-based 3-D PC mostly focus on template structures, which limiting their application. Also, the MOF-based 3-D PCs in most reports were prepared *via* a method highly relevant to their own characteristics. Therefore, a general method for the preparation of MOF films is still lacking. In addition, due to the need for template manufacturing and removal in the preparation process, the efficiency of the template method to prepare MOFs is low. Accordingly, there have been some attempts to improve the techniques for the fabrication of MOF-based 3-D PCs. F. Huo *et al.*[105] developed a layer-by-layer manufacturing process *via* the Langmuir-Blodgett (LB) technique to prepare 3-D PCs. UIO-66 nanoparticles were chosen due to their large specific surface area and excellent chemical inertness. After a certain number of transfer processes from the water-air interface to the surface of the substrate, UIO-66 3-D PC films were acquired and used for the detection of organic vapor (Fig. 7e). The UIO-66 3-D PC sensor demonstrated large absorption peak shifts for ethanol. In 2017, C. López and D. Maspoch[106] reported a pioneering work on the fabrication of millimetre-sized superstructures. The superstructures were composed of truncated rhombic dodecahedral

Table 2 Comparison of the sensing performances of different MOF-based 3-D PC gas sensors

Components	Target analytes	Sensitivity	Response times (s)	Recovery times (s)	LOD (ppm)	Ref.
HKUST-1/SiO_2	CS_2	16 nm (Saturated vapor)	<10	<10	0.5	100
HKUST-1/PS	Methanol	~9 nm (Saturated vapor)	<10	—	—	101
HKUST-1/PS	Ethanol	9 nm (Saturated vapor)	<30	—	—	103
SiO2/HKUST-1, MOF-5, ZIF-8, MIL-101	Acetone	75 nm (Saturated vapor)	—	—	—	104
UIO-66	Ethanol	30 nm (Saturated vapor)	—	—	—	105
ZIF-8	*n*-BuOH	46 nm (Saturated vapor)	—	—	—	106
RD ZIF-8	*n*-Octane	~55 nm (Saturated vapor)	<350	—	—	109
UIO-66	Ethanol	22.4 nm	2	3	33	110
NR/ZIF-8	Acetone	/	—	—	60	111
ZIF-8/GQDs	Benzene	0.11 nm ppm^{-1}	~1	~7	1	27
ZIF-8	Acetone	32 nm (Saturated vapor)	~7	—	—	112
HKUST-1/SiO_2	Humidity	9 nm	14	17	500	114

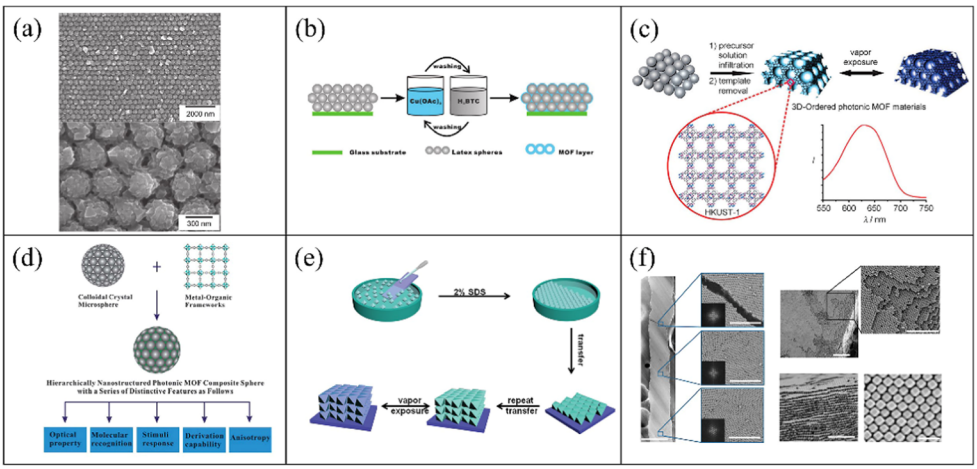

Fig. 7 (a) SEM images of HKUST-1-containing silica 3-D PC vapors sensor. Reproduced with permission.[100] Copyright 2011, Wiley-VCH. (b) Illustration of the fabrication of a HKUST-1-coated PS 3-D PC sensor. Reproduced with permission.[101] Copyright 2011, The Royal Society of Chemistry. (c) Schematic illustration of the preparation of a 3-D inverse opal gas sensor. Reproduced with permission.[103] Copyright 2011, Wiley-VCH. (d) Schematic of the strategy for the preparation of MOF-based PCs spheres. Reproduced with permission.[104] Copyright 2014, The Royal Society of Chemistry. (e) Illustration of the self-assembled MOF-based 3-D PC gas sensors using the LB technique. Reproduced with permission.[105] Copyright 2014, Wiley-VCH. (f) SEM images of self-assembled ZIF-8 3-D PCs without templates. Reproduced with permission.[106] Copyright 2017, Springer Nature.

(TRD) particles of ZIF-8. The superstructures only consisting of ZIF-8 showed the properties of PCs. Fig. 7f shows the SEM images of the superstructure assembled by the ZIF-8 nanoparticles, where a highly ordered array of ZIF-8 nanoparticles can be observed. The superstructures consisting of ZIF-8 exhibited the maximum reflected peak-shift of 46 nm when exposed to *n*-butanol vapor. Moreover, this method for the preparation of superstructures can also be extended to other MOFs such as UIO-66. Therefore, the approach of evaporation-induced self-assembly with simple, convenient, and template-free properties can be a general approach to produce 3-D PCs.

The physicochemical performances of crystals are distinct because of the interaction between atoms and the different bond distances along the crystal direction.[107] Therefore, the adsorption characteristics of MOF films can be improved by changing the orientation of the crystals on the MOF surface. D. Maspoch *et al.*[108] presented an evaporation-induced self-assembly method to fabricate superstructures. The superstructures could have different crystal plane orientations by adjusting the surfactant content. By adding a variable content of cetyltrimethylammonium bromide (CTAB), (111)-, (100)-, and (110)-oriented face-centered cubic 3-D PCs consisting of ZIF-8 were obtained. The ZIF-8 superstructures exhibited distinct optical properties due to the variation in their crystal plane orientation, which may facilitate an enhancement in the sensing performances of MOF-based PC sensors. D. Chen *et al.*[109] further investigated the sensing properties of MOF-based 3-D PC sensors with different grain boundaries and crystal facets. They found that the exposed crystal facets can obviously influence the selectivity of ZIF-8-based 3-D PCs to chemical vapor *via* diffusion regulation. RD ZIF-8 3-D PCs with one exposing crystal facet of (110) showed distinguished selectivity for C5–C8 linear alkanes, C6–C8 linear alkenes and C1–C8 linear alcohols. The sensing system of the RD ZIF-8 3-D PC film successfully realized the detection of the gasoline octane number. Besides the grain boundaries and crystal facets, the sizes and defects of the building blocks also have an effect on 3-D ordered structures. G. Lu and H. Yu *et al.*[110] investigated the influence of crystal size and missing-linker defects on the sensing properties of PC films assembled by UIO-66 nanoparticles. The tuning and optimization of the crystal sizes and missing-linker defects could obviously enhance the sensitivity, response and recovery of the MOF-based 3-D PC sensors. In addition, the combination of MOF-based 3-D PCs and other advanced materials is a promising way to improve the sensing performance of the detection system. C. M. Doherty and R. A. Caruso[111] proposed an approach to enhance the fluorescence signal for organic vapor detection through the combination of MOF-based superstructures and fluorescent organic dyes. The overall fabrication process is shown in Fig. 8a. The PC film assembled using ZIF-8 nanoparticles and Nile red demonstrated a 200-fold fluorescence intensity compared with the disordered film consisting of ZIF-8. The reason for this enhancement in fluorescence may be the resonance when the fluorescence wavelength is near the PBG of 3-D PCs. Through a variation in fluorescence intensity or shift in its reflection spectrum, the sensing system exhibited excellent selectivity among aromatic homologs and distinguished sensitivity for acetone. Y. Chen *et al.*[27] presented a method for the preparation of a template-free 3-D PC benzene sensor assembled by ZIF-8@graphene quantum dots (GQDs). As depicted in Fig. 8b, the sensing system showed excellent selectivity for benzene and a low LOD of 1 ppm because of the porosity characteristic of ZIF-8 and the π–π stacking interactions.

In addition, J. Zhang and H. Duan[112] presented an approach for the preparation of amorphous photonic structures consisting of spherical/polyhedral MOF nanoparticles. Amorphous photonic structures, which have isotropic structural colors, are suitable for

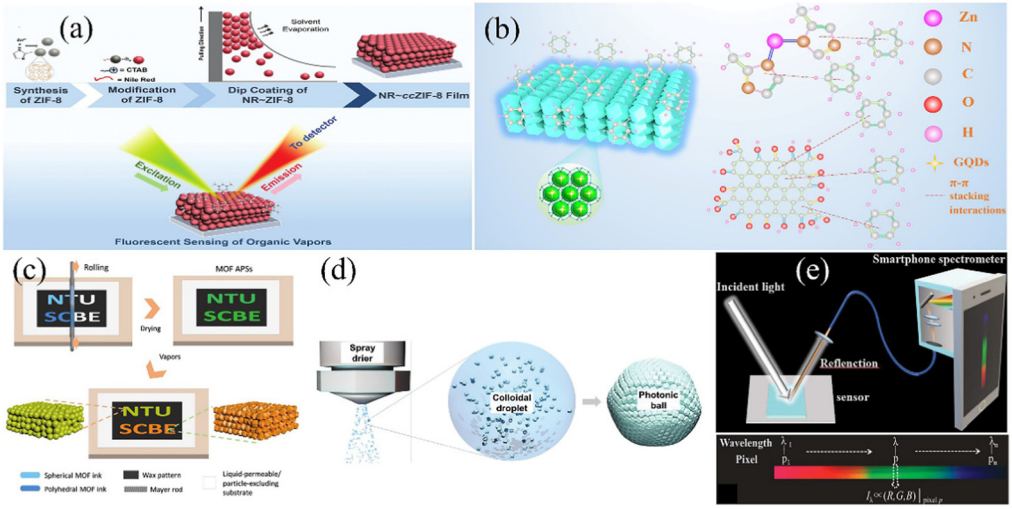

Fig. 8 (a) Schematic illustration of the fabrication and fluorescent sensing by NR ~ ZIF-8 3-D PC gas sensor. Reproduced with permission.[111] Copyright 2020, Wiley-VCH. (b) Schematic diagram of ZIF-8@GQD 3-D PC benzene sensor. Reproduced with permission.[27] Copyright 2021, The Royal Society of Chemistry. (c) Preparation route of ZIF-8 amorphous photonic structures with an infiltration-assisted Mayer rod coating technique. Reproduced with permission.[112] Copyright 2019 Wiley-VCH. (d) Schematic illustration of the self-assembly of MOF-based PC spheres by spray drying. Reproduced with permission.[113] Copyright 2021, Wiley-VCH. (e) Scheme of the combination of a HKUST-1-based 3-D PC sensor and a smartphone spectrometer. Reproduced with permission.[114] Copyright 2020, IEEE.

constructing sensing elements with different shapes. They utilized an approach of infiltration-assisted Mayer rod coating to develop customized patterns of ZIF-8 amorphous photonic structures (Fig. 8c). A sensing array consisting of ZIF-8 amorphous photonic structures was further produced to realize the detection of organic vapor. Similarly, as illustrated in Fig. 8d, M. Faustini *et al.*[113] demonstrated the fabrication of MOF photonic spheres with amorphous photonic structures *via* a spray-drying approach, which was inexpensive with high throughput. This method for the preparation of MOF photonic balls shows versatility, which has great promise in the application of chemical sensing. Moreover, the integrated system of 3-D PC sensors and smart equipment may also be a step forward. H. Ding *et al.*[114] developed a composite 3-D PC humidity sensor, in which the sensing signal could be detected by a smartphone (Fig. 8e). A smartphone can be established as a spectrometer through the integration of its camera and a simple dispersive element. The smartphone spectrometer could expediently detect the sensing signal of the structural color variation, which established a lab-on-phone platform for the detection of humidity.

Summary and outlook

During the last decade, there has been increasing interest in MOF-based PC sensors due to their distinct structures and versatile properties. Also, neither functionalization at the molecular level nor complex transformation and detection of the sensing signal are necessary, and thus they have wide application prospect in the sensing field. Moreover, the anti-electromagnetic interference and high-reliability properties of MOF-based PC sensors enable their general application in the chemical, physical and biological fields. This review summarized the literature on MOF-based PCs as label-free gas/vapor sensors and examined their corresponding sensing mechanism, material selection, structural optimization and sensing performances from the perspective of 1-, 2-, and 3-D PCs. We also presented a general survey of the development of MOF-based PC gas/vapor sensors, aiming to open up a broader prospect of constructing PC sensors with outstanding properties. At present, there are two ways to improve the sensing performances of MOF-based PC gas/vapor sensors. The first is to optimize the MOF materials used as the building blocks of PCs. This includes the selection of MOFs, the sizes and shapes of MOF nanoparticles, the number of defects, and their combination with other sensitive materials. The second is the optimization of PC structures, including their layer number, thickness, and overall shape. In theory, the optical features of 1-D PCs improve with an increase in the number of cycles. However, this is not the case in real situations. Thus, the optimization of the number of cycles is significant for the sensing performances. The thickness and overall shape of MOF-based PC sensors may be related to their response speed. This problem needs to be further studied.

Overall, the research in PC gas sensors based on MOFs is still in its infancy compared with other types of sensors. They also face a series of challenges and need further studies and investigations. These challenges in the development of PC gas sensors based on MOFs are discussed as follows:

(1) A drawback of MOF-based PC sensors is the concentration-dependent characteristic of the effective refractive index of the MOF layers, which causes the inadequacy of MOF-based PC sensors to recognize guest molecules accurately. Although some MOF-based PC sensors with innovative structures and unique optical characteristics have been presented, it is still necessary to improve the tuning range and response rate of PC systems. For example, besides the inherent properties of materials (such as

elasticity and swelling capacity), it is also important to select/prepare suitable MOF materials for further improving the specificity of MOF-based PC gas sensors.

(2) Although MOFs have multiple advantages compared to other sensing materials, a major drawback is their poor stability, especially chemical inertness and hydrolytic stability. These defects continue to inhibit their promotion to the level of practical implementation. In addition, another pertinent challenge in the real-time applicability of MOFs as gas/vapour sensors is their ability to adsorb water. The presence of moisture can substantially hinder the sensitivity and response time. At present, MOF-based PC sensors usually are assembled by some MOFs with long stability and hydrophobicity to avoid this problem. Thus, researchers have to find new approaches such as surface modification and synthesis of new MOFs to overcome this inadequacy.

(3) The sensing signals of MOF-based PC gas sensors are mainly the shifts in their reflected peaks due to the variation in their refractive index. Thus, isomerides or analytes with the same refractive index cannot be distinguish well. Moreover, in a realistic detection scenario, the analyte is often not a single gas but a mixture of gases. Single MOF-based PC gas sensors always exhibit poor selectivity. The solution to this question is the construction of photonic nose chips, which are sensing arrays consisting of multiple sensors with unique composite sensing responses for different analytes. In addition, combined with the artificial intelligence for data processing and machine learning research, intelligent photonic nose chips can be produced for better detection.

(4) In practical sensing applications, sensors must achieve miniaturized program, extended function, and simplified operation. This raises the need for preparing sensing systems combining smart mobile devices such as smart phones, tablet personal computers, personal digital assistants, smart bands, unmanned aerial vehicles and intelligent robots.

In summary, due to the high reliability, low power consumption, and adjustable characters of MOF-based PC gas sensors, they exhibit a great utilization potential. With persistent efforts from researchers, we believe that MOF-based PC gas sensors can establish a pivotal position in the field of gas sensing.

Conflicts of interest

There are no conflicts to declare.

Acknowledgements

This work was supported by the National Natural Science Foundation of China (Grant No. 61875235).

References

1 R. V. Nair and R. Vijaya, *Prog. Quant. Electron.*, 2010, **34**, 89–134.
2 X. Liu, S. Cheng, H. Liu, S. Hu, D. Zhang and H. Ning, *Sensors*, 2012, **12**, 9635–9665.
3 L. E. Kreno, K. Leong, O. K. Farha, M. Allendorf, R. P. Van Duyne and J. T. Hupp, *Chem. Rev.*, 2012, **112**, 1105–1125.
4 H. Xu, P. Wu, C. Zhu, A. Elbaz and Z. Z. Gu, *J. Mater. Chem. C*, 2013, **1**, 6087–6098.
5 J. Zhou, C. Zeng, H. Ou, Q. Yang, Q. Xie, A. Zeb, X. Lin, Z. Ali and L. Hu, *J. Mater. Chem. C*, 2021, **9**, 11030–11058.
6 M. E. Calvo, S. Colodrero, N. Hidalgo, G. Lozano, C. López-López, O. Sánchez-Sobrado and H. Míguez, *Energy Environ. Sci.*, 2011, **4**, 4800–4812.
7 L. Wang, *Sens. Actuators, A*, 2020, **307**, 111984.
8 A. Gheorghe, O. Lugier, B. Ye and S. Tanase, *J. Mater. Chem. C*, 2021, 16132–16142, DOI: **10.1039/d1tc02249k**.
9 M.-L. Hu, S. A. A. Razavi, M. Piroozzadeh and A. Morsali, *Inorg. Chem. Front.*, 2020, **7**, 1598–1632.
10 X. Guo, Y. Ding, D. Kuang, Z. Wu, X. Sun, B. Du, C. Liang, Y. Wu, W. Qu, L. Xiong and Y. He, *J. Colloid Interface Sci.*, 2021, **595**, 6–14.
11 A. Buragohain and S. Biswas, *CrystEngComm*, 2016, **18**, 4374–4381.
12 Y. Wang, L. Yao, L. Xu, W. Wu, W. Lin, C. Zheng, Y. Feng and X. Gao, *Sens. Actuators, B*, 2021, **332**, 129497.
13 Y. Belmabkhout, P. M. Bhatt, K. Adil, R. S. Pillai, A. Cadiau, A. Shkurenko, G. Maurin, G. Liu, W. J. Koros and M. Eddaoudi, *Nat. Energy*, 2018, **3**, 1059–1066.
14 X. Chen, T. Wang, Y. Han, W. Lv, B. Li, C. Su, M. Zeng, J. Yang, N. Hu, Y. Su and Z. Yang, *Sens. Actuators, B*, 2021, **345**, 130423.
15 X. Chen, S. Wang, C. Su, Y. Han, C. Zou, M. Zeng, N. Hu, Y. Su, Z. Zhou and Z. Yang, *Sens. Actuators, B*, 2020, **305**, 127393.
16 X. Chen, T. Wang, J. Shi, W. Lv, Y. Han, M. Zeng, J. Yang, N. Hu, Y. Su, H. Wei, Z. Zhou, Z. Yang and Y. Zhang, *Nanomicro Lett.*, 2021, **14**, 8.
17 S. Qin, L. Qu, D. Wei, B. C. Zhang and N. W. Qiu, *Adv. Mater. Res.*, 2011, **301-303**, 497–502.
18 C. Arul, K. Moulaee, N. Donato, D. Iannazzo, N. Lavanya, G. Neri and C. Sekar, *Sens. Actuators, B*, 2021, **329**, 129053.
19 C. Zhang, S. Zhang, Y. Yang, H. Yu and X. Dong, *Sens. Actuators, B*, 2020, **325**, 128804.
20 Y. Xue, S. Zheng, H. Xue and H. Pang, *J. Mater. Chem. A*, 2019, **7**, 7301–7327.
21 C. S. B. Colette McDonagh and B. D. MacCraith, *Chem. Rev.*, 2008, **108**, 400–422.
22 G. Piszter, K. Kertész, Z. Bálint and L. P. Biró, *Sensors*, 2019, **19**, 3058.
23 Z. Ma, T. Yuan, Y. Fan, L. Wang, Z. Duan, W. Du, D. Zhang and J. Xu, *Sens. Actuators, B*, 2020, **311**, 127365.
24 Y. Kang, K. Kim, B. Cho, Y. Kwak and J. Kim, *ACS Sens.*, 2020, **5**, 754–763.
25 Z. Xie, K. Cao, Y. Zhao, L. Bai, H. Gu, H. Xu and Z. Z. Gu, *Adv. Mater.*, 2014, **26**, 2413–2418.
26 S. L. Luo, C. J. Lin, K. H. Ku, K. Yoshinaga and T. M. Swager, *ACS Nano*, 2020, **14**, 7297–7307.
27 Z. Wang, K. Zhan, Y. Zhu, J. Yan, B. Liu and Y. Chen, *Analyst*, 2021, **146**, 7240–7249.

28 Z. Cai, N. L. Smith, J. T. Zhang and S. A. Asher, *Anal. Chem.*, 2015, **87**, 5013–5025.
29 T. Rasheed and F. Nabeel, *Coordin. Chem. Rev.*, 2019, **401**, 213065.
30 Y. Chen, S. Wang, Y. Hu, H. Chen, H. Fu, C. Zhou and Y. She, *Microchem. J.*, 2021, **167**, 106277.
31 M. Arslan, M. Zareef, H. E. Tahir, Z. Guo, A. Rakha, H. Xuetao, J. Shi, L. Zhihua, Z. Xiaobo and M. R. Khan, *Food Chem.*, 2022, **368**, 130783.
32 D. Kou, Y. Zhang, S. Zhang, S. Wu and W. Ma, *Chem. Eng. J.*, 2019, **375**, 121987.
33 P. Lova, C. Bastianini, P. Giusto, M. Patrini, P. Rizzo, G. Guerra, M. Iodice, C. Soci and D. Comoretto, *ACS Appl. Mater. Interfaces*, 2016, **8**, 31941–31950.
34 J. Wang, P. W. H. Pinkse, L. I. Segerink and J. C. T. Eijkel, *ACS Nano*, 2021, **15**, 9299–9327.
35 C. Fenzl, T. Hirsch and O. S. Wolfbeis, *Angew. Chem., Int. Ed.*, 2014, **53**, 3318–3335.
36 F. Qi, Z. Meng, M. Xue and L. Qiu, *Anal. Chim. Acta*, 2020, **1123**, 91–112.
37 K. Zhong, J. Li, L. Liu, S. Van Cleuvenbergen, K. Song and K. Clays, *Adv. Mater.*, 2018, **30**, 1707246.
38 M. Pan, X. b Li, C. Xiong, X. Chen, L. Wang, X. Chen, L. Pan, H. Xu, J. Zhao and Y. Li, *Part. Part. Syst. Charact.*, 2020, **37**, 1900495.
39 Y. Zhang, Y. Qi and S. Zhang, *Adv. Mater. Interfaces*, 2021, **8**, 2100889.
40 D. Men, D. Liu and Y. Li, *Sci. Bull.*, 2016, **61**, 1358–1371.
41 Z. Wang, K. Zhan, Y. Zhu, J. Yan, B. Liu and Y. Chen, *J. Environ. Chem. Eng.*, 2021, **9**, 105445.
42 G. Lu and J. T. Hupp, *J. Am. Chem. Soc.*, 2010, **132**, 7832–7833.
43 J. F. Olorunyomi, S. T. Geh, R. A. Caruso and C. M. Doherty, *Mater. Horiz.*, 2021, **8**, 2387–2419.
44 Y. Y. Li, D. Luo, K. Wu and X. P. Zhou, *Dalton Trans.*, 2021, **50**, 4757–4764.
45 C. Cong and H. Ma, *Adv. Opt. Mater.*, 2021, **9**, 2100733.
46 Y. Feng, Y. Wang and Y. Ying, *Coordin. Chem. Rev.*, 2021, **446**, 214102.
47 K. Okada, M. Nakanishi, K. Ikigaki, Y. Tokudome, P. Falcaro, C. J. Doonan and M. Takahashi, *Chem. Sci.*, 2020, **11**, 8005–8012.
48 V. Stavila, A. A. Talin and M. D. Allendorf, *Chem. Soc. Rev.*, 2014, **43**, 5994–6010.
49 Z. Zhang, K. Muller, S. Heidrich, M. Koenig, T. Hashem, T. Schloder, D. Bleger, W. Wenzel and L. Heinke, *J. Phys. Chem. Lett.*, 2019, **10**, 6626–6633.
50 S. Wang, S. S. Park, C. T. Buru, H. Lin, P. C. Chen, E. W. Roth, O. K. Farha and C. A. Mirkin, *Nat. Commun.*, 2020, **11**, 2495.
51 Q. Fu, Y. Ran, X. Zhang and J. Ge, *ACS Appl. Mater. Interfaces*, 2020, **12**, 44058–44066.
52 L. Li, X. Jiao, D. Chen, B. V. Lotsch and C. Li, *Chem. Mater.*, 2015, **27**, 7601–7609.
53 W. Luo, Y. Zheng, J. Yan and Y. Chen, *ChemistrySelect*, 2019, **4**, 3936–3939.
54 S. Carrasco, *Biosensors*, 2018, **8**, 92.
55 H. Yuan, N. Li, W. Fan, H. Cai and D. Zhao, *Adv. Sci.*, 2022, **9**, e2104374.
56 Z. Zhai, X. Zhang, X. Hao, B. Niu and C. Li, *Adv. Mater. Technol.*, 2021, **6**, 2100127.
57 E. Yablonovitch, *Phys. Rev. Lett.*, 1987, **58**, 2059–2062.
58 S. John, *Phys. Rev. Lett.*, 1987, **58**, 2486–2489.
59 A. Afsari and M. J. Sarraf, *Superlattice Microst.*, 2020, **138**, 106362.
60 W. P. Lustig, S. Mukherjee, N. D. Rudd, A. V. Desai, J. Li and S. K. Ghosh, *Chem. Soc. Rev.*, 2017, **46**, 3242–3285.
61 D. Kou, W. Ma, S. Zhang, J. L. Lutkenhaus and B. Tang, *ACS Appl. Mater. Interfaces*, 2018, **10**, 41645–41654.
62 M. Dantl, S. Guderley, K. Szendrei-Temesi, D. Chatzitheodoridou, P. Ganter, A. Jimenez-Solano and B. V. Lotsch, *Small*, 2021, **17**, 2007864.
63 Z. H. Jia, R. Xie, Y. Qiu, X. B. Lv, X. J. Ju, W. Wang, Z. Liu and L. Y. Chu, *Macromol. Rapid Commun.*, 2021, **42**, 2100200.
64 J. Ge and Y. Yin, *Angew. Chem., Int. Ed.*, 2011, **50**, 1492–1522.
65 H. Yang, L. Pan, Y. Han, L. Ma, Y. Li, H. Xu and J. Zhao, *Appl. Surf. Sci.*, 2017, **423**, 421–425.
66 D. Kou, S. Zhang, J. L. Lutkenhaus, L. Wang, B. Tang and W. Ma, *J. Mater. Chem. C*, 2018, **6**, 2704–2711.
67 K. Zhan, Z. Wang, Y. Zhu, J. Yan and Y. Chen, *Microporous Mesoporous Mater.*, 2021, **323**, 111253.
68 Z. Hu, C.-a Tao, F. Wang, X. Zou and J. Wang, *J. Mater. Chem. C*, 2015, **3**, 211–216.
69 G. Lu, O. K. Farha, W. Zhang, F. Huo and J. T. Hupp, *Adv. Mater.*, 2012, **24**, 3970–3974.
70 F. M. Hinterholzinger, A. Ranft, J. M. Feckl, B. Rühle, T. Bein and B. V. Lotsch, *J. Mater. Chem.*, 2012, **22**, 10356–10362.
71 Z. Hu, C.-a Tao, H. Liu, X. Zou, H. Zhu and J. Wang, *J. Mater. Chem. A*, 2014, **2**, 14222–14227.
72 C. Serre, C. Mellot-Draznieks, S. Surble, N. Audebrand, Y. Filinchuk and G. Ferey, *Science*, 2007, **315**, 1828–1831.
73 A. C. McKinlay, J. F. Eubank, S. Wuttke, B. Xiao, P. S. Wheatley, P. Bazin, J. C. Lavalley, M. Daturi, A. Vimont, G. De Weireld, P. Horcajada, C. Serre and R. E. Morris, *Chem. Mater.*, 2013, **25**, 1592–1599.
74 J. Liu, E. Redel, S. Walheim, Z. Wang, V. Oberst, J. Liu, S. Heissler, A. Welle, M. Moosmann, T. Scherer, M. Bruns, H. Gliemann and C. Wöll, *Chem. Mater.*, 2015, **27**, 1991–1996.
75 A. Ranft, F. Niekiel, I. Pavlichenko, N. Stock and B. V. Lotsch, *Chem. Mater.*, 2015, **27**, 1961–1970.
76 A. von Mankowski, K. Szendrei-Temesi, C. Koschnick and B. V. Lotsch, *Nanoscale Horiz.*, 2018, **3**, 383–390.
77 D. Kou, W. Ma, S. Zhang, R. Li and Y. Zhang, *ACS Appl. Mater. Interfaces*, 2020, **12**, 11955–11964.
78 Y. Xing, L. Shi, J. Yan and Y. Chen, *ChemistrySelect*, 2020, **5**, 3946–3953.
79 K. Zhan, Y. Zhu, J. Yan and Y. Chen, *Phys. Lett. A*, 2020, **384**, 126678.

80 H. Kim, S. R. Rao, E. A. Kapustin, L. Zhao, S. Yang, O. M. Yaghi and E. N. Wang, *Nat. Commun.*, 2018, **9**, 1191.
81 S. Y. Hyunho Kim, S. R. Rao, S. Narayanan, E. A. Kapustin, H. Furukawa, A. S. Umans, O. M. Yaghi and E. N. Wang, *Science*, 2017, **356**, 430–434.
82 K. Zhan, Y. Xing, Y. Zhu, J. Yan and Y. Chen, *Sens. Actuators, A*, 2020, **314**, 112249.
83 N. Sobana and M. Swaminathan, *Sol. Energy Mater. Sol. Cells*, 2007, **91**, 727–734.
84 Y. Xing, Z. Wang, Y. Zhu, J. Yan and Y. Chen, *Phys. Lett. A*, 2021, **400**, 127301.
85 G. Kaur, R. K. Rai, D. Tyagi, X. Yao, P.-Z. Li, X.-C. Yang, Y. Zhao, Q. Xu and S. K. Singh, *J. Mater. Chem. A*, 2016, **4**, 14932–14938.
86 K. Zhan, Z. Wang, Y. Zhu, J. Yan and Y. Chen, *IEEE Sens. J.*, 2021, **21**, 16469–16474.
87 V. V. Pokropivnyi, *Powder Metall. Met. Ceram.*, 2002, **41**, 369–381.
88 F. Parandin, F. Heidari, Z. Rahimi and S. Olyaee, *Opt. Laser Technol.*, 2021, **144**, 107397.
89 J. T. Zhang, Z. Cai, D. H. Kwak, X. Liu and S. A. Asher, *Anal. Chem.*, 2014, **86**, 9036–9041.
90 P. Sharma, Dr. P. Sharan and P. Deshmukh, 2015 International Conference on Pervasive Computing, 2015, DOI: **10.1109/PERVASIVE.2015.7087208**, 1–5.
91 T. Chen, Z.-Y. Deng, S.-N. Yin, S. Chen and C. Xu, *J. Mater. Chem. C*, 2016, **4**, 1398–1404.
92 M. Nankali, Z. Einalou, M. Asadnia and A. Razmjou, *ACS Appl. Bio Mater.*, 2021, **4**, 1958–1968.
93 C. Li, L. Li, S. Yu, X. Jiao and D. Chen, *Adv. Mater. Technol.*, 2016, **1**, 1600127.
94 L. Li, X. Jiao, D. Chen and C. Li, *Cryst. Growth Des.*, 2016, **16**, 2700–2707.
95 O. Dalstein, D. R. Ceratti, C. Boissière, D. Grosso, A. Cattoni and M. Faustini, *Adv. Funct. Mater.*, 2016, **26**, 81–90.
96 A. Razmjou, M. Asadnia, O. Ghaebi, H. C. Yang, M. Ebrahimi Warkiani, J. Hou and V. Chen, *ACS Appl. Mater. Interfaces*, 2017, **9**, 38076–38080.
97 O. Dalstein, E. Gkaniatsou, C. Sicard, O. Sel, H. Perrot, C. Serre, C. Boissiere and M. Faustini, *Angew. Chem., Int. Ed.*, 2017, **56**, 14011–14015.
98 X. Dang, X. Jiang, T. Zhang and H. Zhao, *Chin. J. Chem.*, 2021, **39**, 1706–1715.
99 C. Liu, Y. L. Tong, X. Q. Yu, H. Shen, Z. Zhu, Q. Li and S. Chen, *ACS Appl. Mater. Interfaces*, 2020, **12**, 2816–2825.
100 G. Lu, O. K. Farha, L. E. Kreno, P. M. Schoenecker, K. S. Walton, R. P. Van Duyne and J. T. Hupp, *Adv. Mater.*, 2011, **23**, 4449–4452.
101 Y. N. Wu, F. Li, Y. Xu, W. Zhu, C. A. Tao, J. Cui and G. Li, *Chem. Commun.*, 2011, **47**, 10094–10096.
102 S. Yoon, H. Park and W. Lee, *Lab Chip*, 2021, **21**, 2997–3003.
103 Y. N. Wu, F. Li, W. Zhu, J. Cui, C. A. Tao, C. Lin, P. M. Hannam and G. Li, *Angew. Chem., Int. Ed.*, 2011, **50**, 12518–12522.
104 J. Cui, N. Gao, C. Wang, W. Zhu, J. Li, H. Wang, P. Seidel, B. J. Ravoo and G. Li, *Nanoscale*, 2014, **6**, 11995–12001.
105 C. Cui, Y. Liu, H. Xu, S. Li, W. Zhang, P. Cui and F. Huo, *Small*, 2014, **10**, 3672–3676.
106 C. Avci, I. Imaz, A. Carne-Sanchez, J. A. Pariente, N. Tasios, J. Perez-Carvajal, M. I. Alonso, A. Blanco, M. Dijkstra, C. Lopez and D. Maspoch, *Nat. Chem.*, 2017, **10**, 78–84.
107 N. T. Nesbitt and M. J. Naughton, *Ind. Eng. Chem. Res.*, 2017, **56**, 10949–10957.
108 C. Avci, Y. Liu, J. A. Pariente, A. Blanco, C. Lopez, I. Imaz and D. Maspoch, *Small*, 2019, **15**, 1902520.
109 S. Yu, X. Wang, X. Jiao, C. Li and D. Chen, *J. Mater. Chem. C*, 2021, **9**, 5379–5386.
110 R. Zhang, D. Zhang, Y. Yao, Q. Zhang, Y. Xu, Y. Wu, H. Yu and G. Lu, *ACS Appl. Mater. Interfaces*, 2019, **11**, 21010–21017.
111 J. F. Olorunyomi, M. M. Sadiq, M. Batten, K. Konstas, D. Chen, C. M. Doherty and R. A. Caruso, *Adv. Opt. Mater.*, 2020, **8**, 2000961.
112 L. Bai, Y. He, J. Zhou, Y. Lim, V. C. Mai, Y. Chen, S. Hou, Y. Zhao, J. Zhang and H. Duan, *Adv. Opt. Mater*, 2019, 1900522, DOI: **10.1002/adom.201900522**.
113 C. Avci, M. L. De Marco, C. Byun, J. Perrin, M. Scheel, C. Boissiere and M. Faustini, *Adv. Mater.*, 2021, **33**, 2104450.
114 C. Chen, H. Ding, Y. Yue and C. Han, *IEEE Photonics Technol. Lett.*, 2020, **32**, 1469–1472.